https://doi.org/10.1016/j.jsv.2021.116401

Broadband and Low Frequency Sound Absorption by Sonic Black Holes with Micro-Perforated Boundaries

Xiaoqi Zhang [a] and Li Cheng [b,*]

[a]School of Energy and Power Engineering, Wuhan University of Technology, Wuhan 430063, China

[b]Department of Mechanical Engineering, The Hong Kong Polytechnic University, Kowloon, Hong Kong, China

[*] Corresponding author.
Email address: li.cheng@polyu.edu.hk

Abstract

Acoustic black holes (ABHs) have been so far investigated mainly for flexural wave manipulation in structures. Exploration of ABHs for sound wave manipulation, referred to as Sonic black holes (SBHs), as well as the design of SBH-based noise control devices are scarce. To fill the gap, this paper proposes a SBH sound absorber inside a circular duct in conjunction with the use of Micro-perforated panels (MPPs) to achieve broadband and low-frequency sound absorption. Capitalizing on the ABH-specific wave retarding and trapping phenomena and the energy dissipation ability of the MPP, a compact and ultra-broadband near perfect sound absorbing device with sub-wavelength thickness is realized for noise abatement in a duct. Finite element simulations are performed to assess the achieved sound absorption performance, which is experimentally confirmed by impedance tube tests. Analyses reveal that the physical mechanism underpinning the superior sound absorption is attributed to the combined effects of the ABH-induced wave speed changes, energy trapping and the spatially graded local resonances of the cavity-backed MPP. The proposed solution shows promise for circumventing some existing limitations of traditional noise control devices.

Keywords: Acoustic black hole; Sonic black hole; Wave retarding and trapping; Micro-perforated panels; Low and ultra-broadband perfect sound absorption.

1. Introduction

Developing sub-wavelength thickness materials/structures for effective low frequency and broadband sound absorption has always been a great challenge in noise control engineering. Conventionally used sound absorption materials, like porous or fibrous materials, are efficient mostly at high frequencies. Their performance deteriorates for low frequency noise when the acoustic wavelength becomes significantly larger than the allowable material/structural thickness. The use of a large amount of materials might be a solution, but this obviously leads to a bulky system which is unacceptable for limited space. To tackle the problem, extensive efforts have been devoted to exploring innovative ideas to develop compact solutions while achieving low-frequency and broadband noise attenuations. One effective approach is the use of space coiling or labyrinthine structures to increase the effective structural thickness and to shrink bulky structures into deep subwavelength scale [1-4]. Another popular option is to use the slow sound phenomenon to decrease the physical thickness of the structure [5-9]. However, most of the existing research focuses on the combination of these effects with Helmholtz resonators or quarter wavelength tubes, and the resulted absorption bandwidth is usually narrow.

Acoustic Black Hole (ABH) phenomenon, a much newer concept, resides in a wave guide which enables wave speed modulation, energy trapping and absorption. A proper ABH design would entail the decay of the phase velocity of the waves, theoretically to zero with the propagation distance. As a result, incident waves would take an infinite amount of time to reach the boundary, thus annulling any energy reflections from there.

This results in an energy accumulation, which can then be trapped around ABH termination and dissipated with a reasonable amount of absorption. This phenomenon is analogous to the term “black hole” used in astrophysics [10-12]. ABHs have received great attention for flexural wave manipulation inside a vibrating structure with its thickness tailored according to a power-law relationship [13-16], particularly for passive structural vibration controls [17, 18], sound radiation [19, 20] and energy harvesting [21-23]. A useful compendium can be found in a recently published review paper [24].

Comparatively, the sonic counterpart of the structural ABH concept, referred to as Sonic Black Hole (SBH), is much less exploited, except for a few exploratory works [25-32]. The first work on SBH was presented in [25], in which sound propagation in a one-dimensional waveguide with a varying cross section and varying acoustic admittance of the walls was theoretically investigated. The existence of the SBH effects was theoretically demonstrated by installing a series of rings with a power-law decaying inner radius in a duct. The reported phenomenon did not receive much attention until many years later, when the interest in the topic resurged. This includes some experimental investigations of the SBH phenomena based on the configuration proposed in Ref. [25] for sound absorption in air [27, 28]. Results show a significant reduction of the acoustic wave reflection arising from the SBH design. From the modeling and analysis perspective, the transfer matrix method [29, 30] has been proposed to model the SBH structure, which allows the examination of the effects of

various parameters on the SBH phenomena. More recently, the application of fractional order operators as an alternative method to model the acoustic black hole terminations in ducts is investigated [31]. Despite the increasing efforts, SBHs for sound absorption are much less researched as compared with their structural counterparts. The application of SBH principles in conceiving practical noise control devices is also lacking.

The materialization of effective SBH phenomena stems from the combined effects of the retarding configuration of the SBH design and effective energy dissipation. Knowing air damping is usually weak, alternatives based on other energy dissipation mechanisms should be envisaged, and this without compromising the SBH-specific decelerating wave propagation. One of the options, to be examined in the present study, is to use a Micro-perforated panel (MPP) as the inner liner in a SBH duct. A MPP is a thin sheet perforated with small holes. With the diameter of the perforated holes typically in sub-millimeter range, the panel itself offers high acoustic resistance and low acoustic reactance, which warrants excellent broadband sound absorption without using any conventional porous or fiber materials. As one of the most promising next generation sound absorption materials, MPP has received extensively attention in acoustic community for various acoustic applications [33-35].

Referring the sonic counterpart of the vibrational ABH as Sonic Black Hole (SBH), we investigate the above issue in the present paper by proposing a SBH sound absorber inside a circular duct in conjunction with the use of a Micro-perforated facing. The target is to achieve enhanced SBH phenomena and meanwhile to realize low and

ultra-broadband sound absorption. More specifically, capitalizing on the SBH features arising from the design and the broadband sound absorption ability of the MPPs, we numerically and experimentally demonstrate a compact, ultra-broadband and near perfect sound absorbing device with sub-wavelength thickness. Quantitatively, the proposed device entails more than 96% of the acoustic energy absorption roughly starting from a frequency, typically in the range $c_0/6L$ □ $c_0/8L$ Hz, and then keeps high absorption level for a broadband frequency range, where c_0 is the sound speed and L is the length of the device. For the configuration used in the paper, the lower limit for 0.5 absorption corresponds to a structural thickness of $\lambda/10$ where λ is the acoustic wavelength. So this can be regarded as a sub-wavelength device. The realized prototype is thus acoustically 'dark' to cover an ultra-broadband frequency range up to 3000 Hz, which is the upper frequency limit investigated in this paper.

The remaining part of the paper is organized as follows. The designed SBH sound absorbing device as well as the finite element model employed to assess its performance are first illustrated in section 2. Analyses are then conducted in section 3 to scrutinize the physical mechanisms underpinning the superior sound absorption performance of the proposed absorber. In section 4, experiments are carried out by impedance tube tests to confirm the numerically predicted sound absorption performance, before major conclusions are summarized.

2. SBH Sound Absorber Model

2.1. Conceptual design model

The basic SBH configuration suggested in [25] is employed as a benchmark to achieve the ABH effects in terms of retarding waves and sound absorption. The system under consideration consists of a set of rings with varying radius mounted on the inner wall of a perfectly hard cylindrical tube of radius R and length L. The inner radius of the rings decreases following a linear power law function: $r(x)=\frac{R}{L}x$, in which x denotes the longitudinal position of the cross section. Such a SBH structure is referred to as Linear Sonic Black Hole (LSBH). The waveguide is thus partitioned by a series of rings, along the inner edges of which, a micro-perforated panel/facing is installed as a liner, as shown in Fig. 1, aiming at maintaining the desired SBH effects while enhancing the energy dissipation. The proposed design creates a series of partitioned air cavities with gradually increasing depth formed by each pair of adjacent rings behind the MPP. This is expected to create graded local resonances of the MPP-backing cavity assembly, conducive to absorbing sound energy at different frequencies, as to be demonstrated later on. The MPP is characterized by its perforated hole diameter d, perforation ratio δ and panel thickness t. In the modelling, the acoustic impedance of the MPP, Z_{MPP}, can be derived using classical Maa's formula [33] as

$$Z_{\mathrm{MPP}}=R+\mathrm{j}\chi, \tag{1a}$$

$$R=\frac{32\mu t}{\delta d^2}\left[\left(1+\frac{K^2}{32}\right)^{\frac{1}{2}}+\frac{\sqrt{2}}{32}K\frac{d}{t}\right], \tag{1b}$$

$$\chi=\frac{\rho\omega t}{\delta}\left[1+\left(9+\frac{K^2}{32}\right)^{-1/2}+0.85\frac{d}{t}\right]. \tag{1c}$$

where $\mathrm{j}=\sqrt{-1}$; $K=\frac{d}{2}\sqrt{\rho\omega/\mu}$ is a parameter describing the ratio of the radius to the viscous boundary layer thickness inside the hole; ρ the density of air; μ the air dynamic viscosity; ω the angular frequency. The real part R is the acoustic resistance which is associated with the acoustic energy dissipation due to viscous effects. The imaginary part χ is referred to as the acoustic reactance, which represents the inertial effects. It should be noted that Eq. (1) only applies to MPPs without flow under a reasonably low acoustic excitation level, valid for linear acoustic regime.

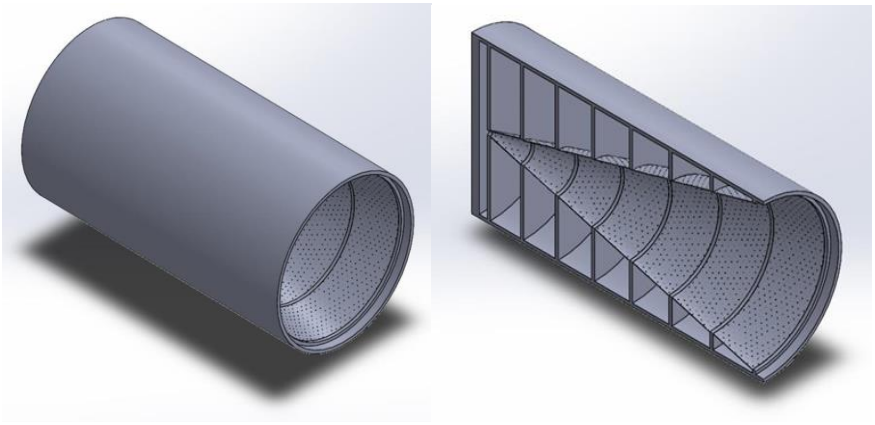

(a) (b)

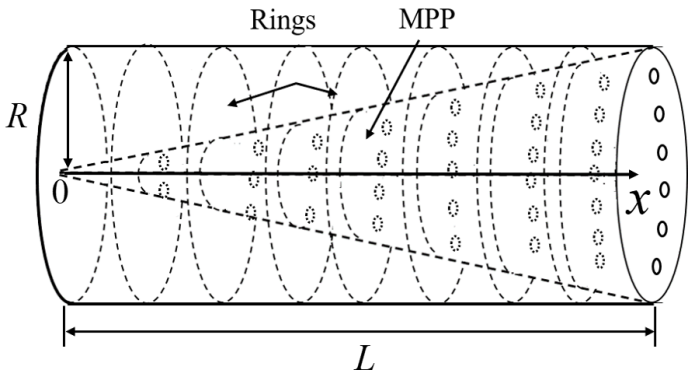

(c)

Figure 1: Conceptual view of the proposed acoustic device showing (a) the overall structure and (b) detailed inner structure with rings and MPP facing. (c) Sketch of the LSBH system with inner MPP facing showing the geometric variables.

2.2. Analysis model

The proposed LSBH device is to be installed as a termination in a circular duct, subject to an incoming acoustic plane wave from its right-hand side (thick end). Finite Element Method (FEM) is adopted to evaluate the acoustic performance of the proposed device using commercial software COMSOL. The thickness of the rings is neglected in the FEM model. Two-microphone transfer function method is employed to obtain the sound absorption coefficient of the designed structure. The analysis frequency range is constraint by the plane wave assumption, specified in Eq. (2) below and the distance between the two microphones S through Eq. (3):

$$f \le \frac{0.58 c_0}{D} \quad , \tag{2}$$

$$\frac{0.05 c_0}{S} \le f \le \frac{0.45 c_0}{S} , \tag{3}$$

where D is the diameter of the duct. Acoustic analyses are conducted after adopting a refined meshing scheme following the general rule of ensuring a minimum of six elements per wavelength in order to capture the fine details of the acoustic wave fluctuation. Air damping is considered in the current study by means of a complex sound speed $c = c_0(1 + 0.05j)$. The inlet section of the duct represents the boundary condition of the acoustic radiating surface with incident acoustic plane waves of 1 P_a in amplitude. Also over the same surface, a plane wave radiation condition in the

opposite direction is imposed. The MPP liner is treated as a impedance surface with impedance Z_{MPP} described by Eq. (1).

3. Results and discussions

3.1. Sound absorption performance

Numerical calculations of sound absorption coefficient of the proposed device are conducted with the following parameters: $R = 25$ mm , $L = 300$ mm , $S = 50$ mm $d = t = 0.2$ mm and $\delta = 1\%$. Fifteen rings are installed inside the LSBH structure. The first ring, with the smallest inner ring diameter, is separated from the acoustically hard backing end by a distance 10 mm. Other fourteen rings are equally spaced inside the structure with a separating distance of 20 mm between each pair of adjacent rings.

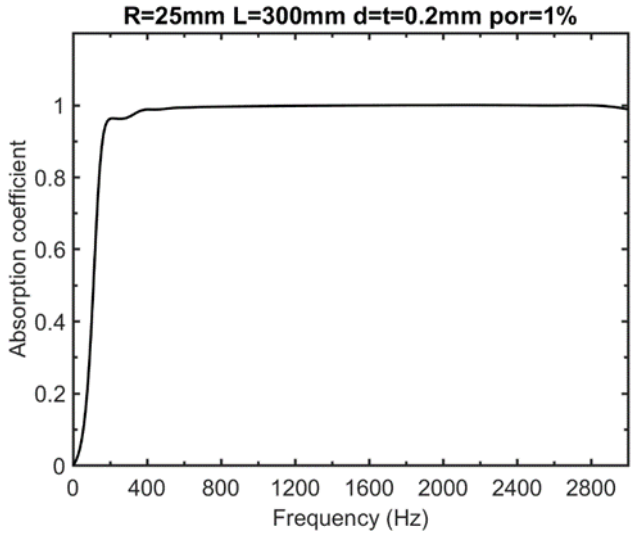

Figure 2: Sound absorption coefficient of the designed system.

Calculated sound absorption coefficient is shown in Fig. 2, showing a sharp increase to 0.96 at around 200 Hz $\approx \frac{c_0}{6L}$, then dowelling around 1 until 3000 Hz in a rather flat and persistent manner. This demonstrates the excellent broadband sound absorption ability of the device, starting from a relatively low frequency. As an

indicative measure, the 0.5 sound absorption bandwidth (defined as the bandwidth corresponding to a sound absorption coefficient above 0.5) actually starts at as low as 110 Hz. With $L = 300$ mm and an acoustic wavelength λ at 110 Hz, the LSBH length is roughly λ/10, which can be regarded as a subwavelength acoustic device. Considering the fact that the absorption coefficient is greater than 0.96 starting from 200 Hz, the designed absorber is thus capable of achieving near perfect absorption in a rather low and broadband frequency region. The most interesting feature of the designed structure is that after the threshold frequency of 200 Hz, the absorption coefficient maintains a very high and persistent level towards high frequencies. Such behavior is different from most traditional resonant based absorbers, whose effective frequency is closely related to the resonances embedded in the absorber and only spans over a very narrow frequency band most of time.

3.2 Sound absorption mechanism and its inherent relationship with SBH effects

In order to gain the physical understanding on the observed absorption features, the sound absorption mechanism is explored. Traditionally, a MPP with a backing cavity forms a so-called MPP absorber, whose effectiveness depends on the resonant behavior of the MPP-backing cavity assembly, which in turn depends on various geometrical parameters of the system relating to both MPP and the backing cavity. As a rough approximation, the designed system can actually be regarded as a series of MPP absorbers with different/graded backing cavity depths D_c, which are connected in parallel along the duct, as shown in Fig. 3. The backing cavity depths of the absorber

units decrease along the axial direction and the resonance frequency of each MPP absorber unit thus depends on the backing cavity depth at its specific location. In the present case, the gradual changes in the cavity depth produce a continuous change of the resonant frequencies in the series of absorber units, gradually reducing towards the end of the SBH duct. To demonstrate this, the absorption curves from each MPP absorber unit obtained through Eq. (4) are plotted in Fig. 4 with corresponding resonance frequencies marked as f_n. Note f_n is calculated using the nominal and constant sound speed in air, i.e. 340 m/s. Due to the cascade effect of this resonance frequency and the overlapping of effective working frequency range of MPP absorbers, the structure as a whole enables rather broadband and flatten near perfect absorption, but in a frequency range which is way above the effective frequency range given by Fig. 2, also reproduced here for better comparison.

$$\alpha = \frac{4R}{\left(1+R\right)^2 + \left(\chi - \cot\left(\omega D_c / c_0\right)\right)^2} \tag{4}$$

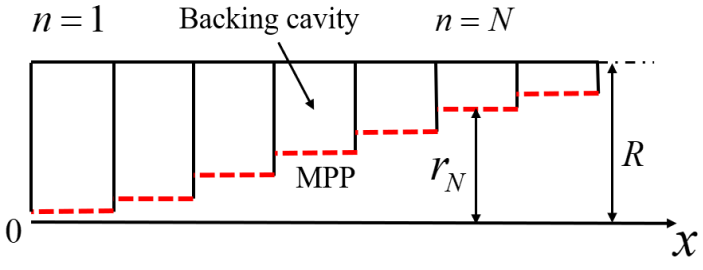

Figure 3: Simplified approximation of the proposed design.

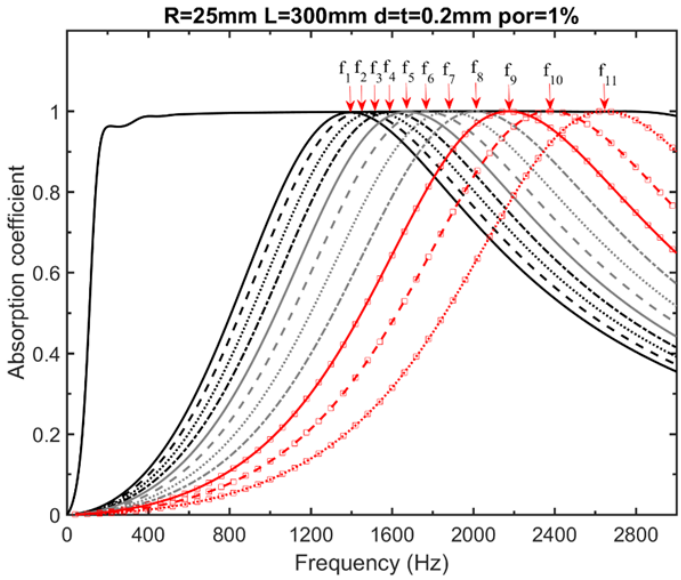

Figure 4: Absorption coefficients and contribution from each of the parallelly connected MPP absorber segment. f_n is calculated using c = 340 m/s.

More specifically, as indicated in Fig. 4, the effective frequency range of these parallel-connected MPP absorber units cannot completely cover the entire effective sound absorption frequency range provided by the LSBH absorber in Fig. 2 since the lowest resonance frequency of the MPP absorber unit is around 1380 Hz. It is clear that the estimation of resonance frequency cascade effect using constant sound speed alone cannot explain such low, broadband and near perfect absorption observed above. To further understand this, the sound pressure distributions inside the duct at different frequencies are plotted in Figs. 5-6. Both figures show that the pressure distribution inside the duct is drastically altered after the wave enters the device, which is quite different from that in the straight duct portion. More specifically, the acoustic wave propagating inside the device is compressed with its wavelength gradually shortened

while reaching the LSBH end. This testifies that the designed structure indeed generates the expected SBH effects in terms of wave compression, evidenced by the sound speed reduction since it is proportional to the wavelength. Meanwhile, the compression of the wave is accompanied by an increase in the sound pressure level, testifying the expected SBH-specific energy concentration phenomenon. In addition, wave energies at different frequencies are concentrated/localized at different positions, analogous to the so-called rainbow-trapping effects. For example, lower frequency energy is more susceptible to be localized at the MPP portion with a deeper backing cavity depth. This goes along with the effective sound absorption range of the absorbers.

To further explain the above, the sound pressure distributions along the middle line (central line of the duct) and the top line (wall of the duct) of the device, representing the sound pressure in front and behind the MPP are plotted in Fig. 6. Note that a pressure difference across the MPP would be a pre-requisite for sound absorption. Based on this, it can be seen from Fig. 6 that, benefiting from the ABH induced energy concentration and the pressure distribution pattern, a pressure difference across the MPP does occur to different extent depending on the frequency of the incoming waves, so that the acoustic energy can be dissipated by the MPP. Meanwhile, the pressure difference appears in different locations at different frequencies due to the resonance frequency cascade effect, which means the acoustic energy is dissipated by different MPP absorber units at different frequencies.

Due to the ABH-induced sound wave slowing-down effect (both in front of and behind the MPP), the effective depth of the MPP absorber backing cavity is in fact

increased as a result of the reduced sound speed. This leads to the down shifting of the resonance frequencies of each absorber unit. By the same token, low frequencies corresponding to long acoustic wavelength which initially fall beyond the working frequency region of the serially connected MPP absorbers are now inside their working frequency region, thus creating more favorable frequency matching with the effective region of these absorber units. For example, Fig. 6 shows that the wavelength at 1000 Hz is shortened from 0.34 m to roughly 0.18 m, the sound speed is thus slowed down from c_0 to $\frac{0.18}{0.34}c_0 \approx 0.53c_0$. Therefore, the time for the sound wave to propagate in the depth direction in the backing cavity nearly doubles, also suggesting a doubling in the effective depth of the backing cavity behind the MPP absorber unit. As shown later, the sound absorption for this frequency component is predominantly from the 9th MPP unit. Sure enough, from a rule of thumb calculation, the original resonance frequency of this unit (2014 Hz) is now down shifted by 0.18/0.343 due to the slow sound induced effective backing cavity depths increasement, namely 1057 Hz, which is much closer to 1000 Hz.

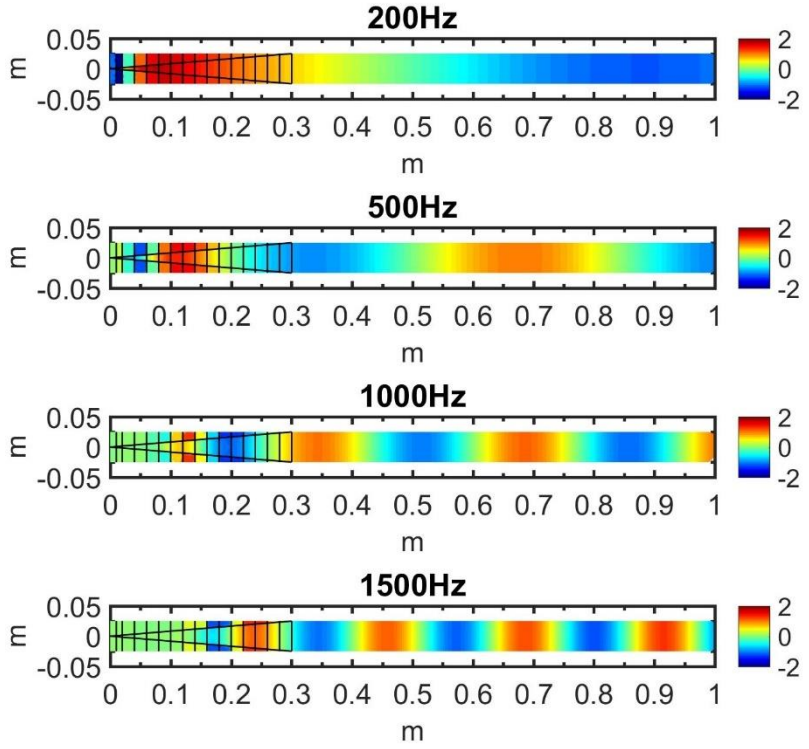

Figure 5: Sound pressure distribution along the middle plane of the entire system at different frequencies.

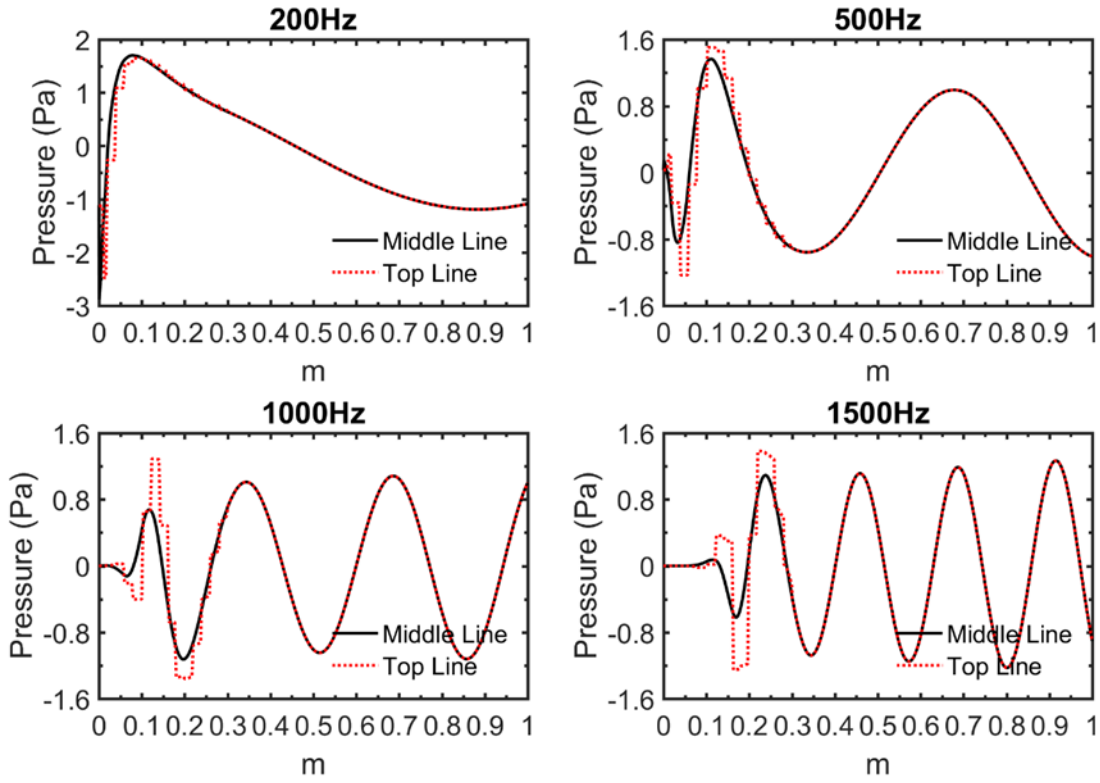

Figure 6: Sound pressure distribution along the middle line (central line of the duct)

and the top line (wall of the duct) of the system at different frequencies.

To further confirm the above explanation, the total power dissipation density physically represents the energy per unit volume in the system dissipated through both the viscous and thermal effects [36-38] at different frequencies are shown in Fig. 7 to quantify the aforementioned energy dissipation process in the system. It is apparent that the energy dissipation mainly occurs in the areas near the MPP so that most of the energy is dissipated by the micro-perforated holes through the viscous effects provided by them. Meanwhile it is clear that the energy dissipation occurs in different areas at different frequencies, more towards the terminating part of the MPP absorber units with a deeper backing cavity depth for lower frequencies, and verse versa. The dominant location for energy dissipation at 1000 Hz is indeed located around the 9th MPP unit which is consistent with the above analysis based on pressure differences and further demonstrates the bandwidth broadening phenomenon induced by the ABH effects.

Therefore, the superior sound absorption performance observed above can be attributed to the favorable sound absorption condition offered to MPP by the SBH effects originating from the SBH plus MPP design. More specifically, the combined ABH wave retarding and energy trapping phenomena, the cascade effect of the MPP absorber units and their resonance frequency down shifting effects together guarantee the excellent low, broadband and near perfect sound absorption of the proposed device.

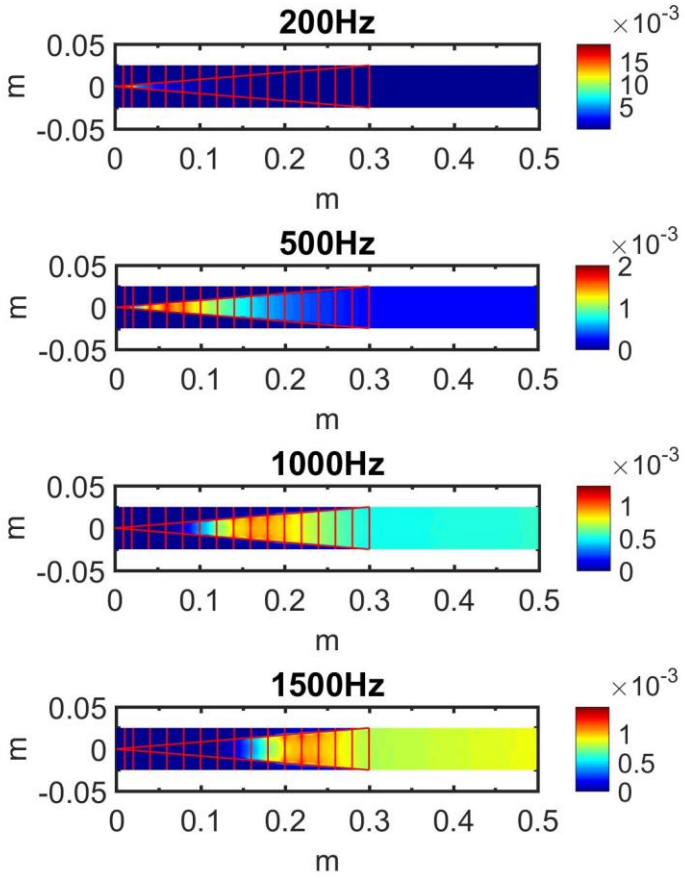

Figure 7: 2D contour of total power dissipation density at the mid-plane of the LSBH at different frequencies. The power dissipation density has a unit of $\mathrm{W/m^3}$.

In practice, the inner radius of the waveguide lined by the MPP may not perfectly decrease to zero as shown in Fig. 8. To take into account possible imperfection in the SBH sound absorber design and implementation, we assume that the inner radius of MPP lined waveguide decreases to a given finite value, rather than zero. As such, the lined MPP is truncated and ends at a finite distance (called truncated length) from the end of the device. More specifically, assume the MPP occupies the region $L - L_{\text{end}} < x < L$, where $L_{\text{end}} > 0$.

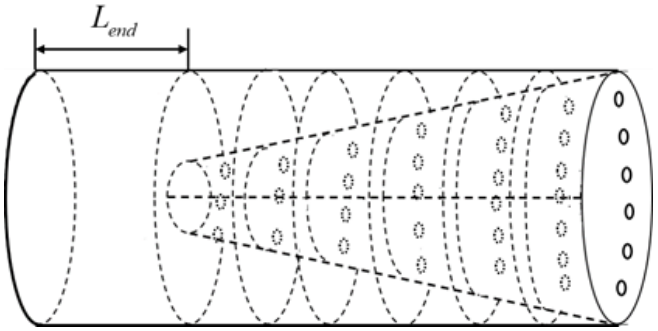

Figure 8: Sketch of the designed acoustic device with a truncated end length.

The influence of the truncated length on the sound absorption is shown in Fig. 9. Note apart from the truncation, other parameters remain the same as before, used in the above simulations. It can be seen that the truncation gives rise to a low absorption trough in the low frequency region, without sensibly affecting the absorption at high frequencies. The resulted absorption curve first oscillates and then remains stable at the same level in the higher frequency region as the ideal case without truncation. The trough gets deeper when the truncation length increases. This is understandable since a larger truncated length would signify a reduced SBH effect. To further understand the appearance of the trough, the sound pressure filed at the trough, 183 Hz, and at two nearby peaks 135 and 253 Hz, for $L_{\text{end}} = 10$ mm is plotted in Fig. 10. It can be observed that, at 183 Hz, the area experiencing a pressure difference across the MPP is the smallest among the three frequencies considered here, which is detrimental to sound absorption. Fig. 9 also shows that increasing the truncation length would shift the locations of the peaks and trough towards a higher frequency alongside a reduction in the sound absorption values. In the worst scenario considered here, an excessive

truncation length would adversely narrow down the 0.5 absorption bandwidth. For example, with L_{end} increased from 10 mm to 40 mm, the locations of the first peak and trough are shifted from 135 to 167 Hz and 183 to 241 Hz, respectively, thus narrowing the 0.5 absorption bandwidth by 110 Hz. Clearly, the existence of the truncation compromises the absorption performance in the low frequency region but does not affect the higher frequencies. This can be explained by the fact that the truncation mainly affects the pressure distribution near the end of the LSBH structure with deeper cavity depths, which are mostly responsible for low frequency absorption. The frequency cascade effects ensure that higher frequency absorption can still be taken care of by those MPP absorber units with shallow backing cavities, located away from the truncated end.

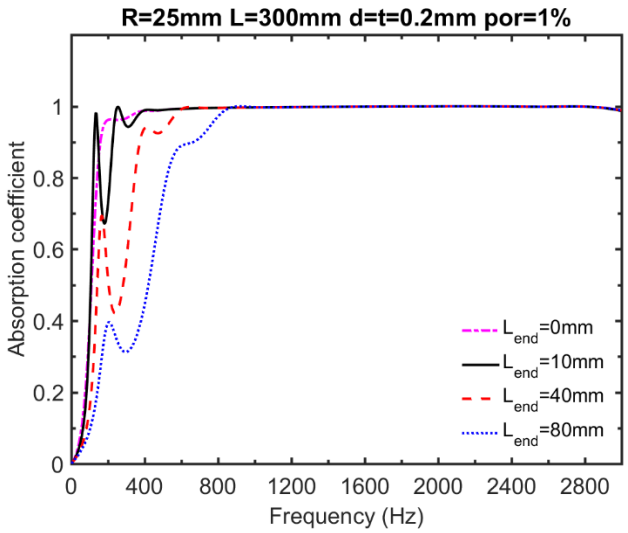

Figure 9: Absorption coefficients of the designed system with different imperfection length L_{end}.

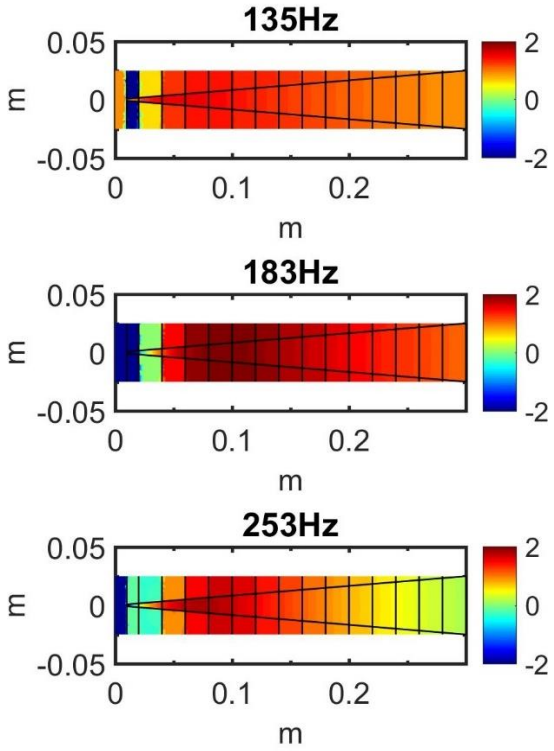

Figure 10: Sound pressure distributions along the middle plane of the whole system at different frequencies when $L_{\text{end}} = 10$ mm.

4. Experimental validation

Experiments are performed on the proposed sound absorber through impedance tube measurement to validate the FEM model and the predicted sound absorption performance of the designed LSBH device. To minimize reflections from possible jumps in the tube diameter, a test sample has been carefully designed, manufactured and assembled with its inner diameter close to that of the impedance tube and the length within the allowable installation region. The geometric parameter of the prototype is thus different from the one used in the preceding analyses. The manufactured LSBH has an inner radius $R = 47.5$ mm and a length $L = 180$ mm. The LSBH structure contains eight rings of 2 mm thick each with their inner radii decaying according to a

linear relationship. The truncation length of the sample is $L_{\text{end}} = 5$ mm, which is also the distance separating the first ring from the duct end. The inter-distance between each pair of rings is 19 mm. The lined MPP, made of aluminum, has a hole diameter $d = 0.2$ mm, thickness $t = 0.2$ mm and perforation ratio $\delta = 1\%$.

The prototype was manufactured by firstly dividing the whole structure into several parts according to the location of the rings. Each part consists of a MPP and a backing cavity. The backing cavities are 3D printed by using ABS resin, as shown in Fig. 11a. All these separate parts are assembled together through glue to form the final prototype.

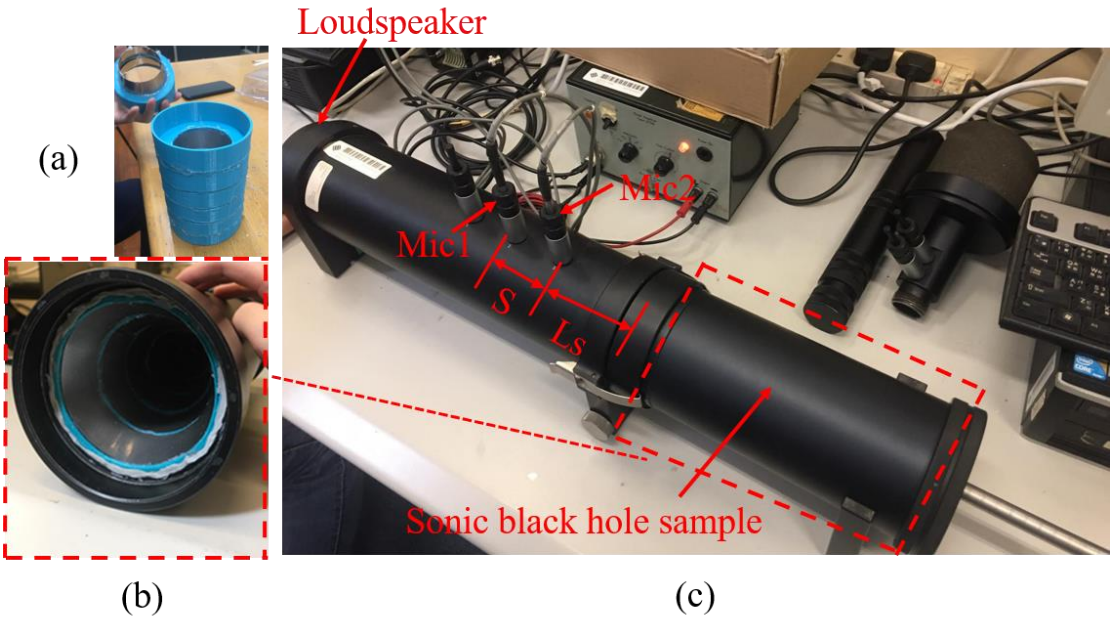

Figure 11: Photograph of the manufactured LSBH sound absorber (a), the test prototype in the sample holder (b) and the sound absorption measurement test rig using impedance tube (c).

As shown in Fig. 11b, the test sample was mounted in a sample holder, which was

then attached to one end of the impedance tube. Two microphones, $S = 50$ mm apart, were flush mounted on the tube, upstream the sample to separate the incident and reflected sound waves in the tube. The selected spacing between the sample and the nearest microphone was $L_s = 100$ mm. While white noise excitation was used for higher frequency measurement (above 400 Hz), single frequency excitation was used for low frequency measurement to enhance the signal-to-noise ration. Figure 11c shows the test rig for sound absorption measurement, including the impedance tube with the installed microphones. The SBH sample was fixed to the end of the tube, with a zoom-in photo showing more details. The two-microphone transfer function method was applied to obtain the absorption coefficient.

The measured and calculated absorption coefficients are compared in Fig. 12. Good agreement is observed between the experimental measurements and the simulation results in terms of both the general trend and the magnitude. The experimental curve shows that the 0.5 absorption bandwidth starts at as low as 165 Hz. With $L = 180$ mm and an acoustic wavelength λ at 165 Hz, the LSBH length is roughly λ/10 which further demonstrates the subwavelength feature of the device. Major phenomena predicted by numerical simulations are basically confirmed, including the oscillation in the low frequency region caused by the truncated end length, the sharp increase to near 1 at very low frequency 230 Hz $\approx \frac{c_0}{8L}$, and the persistent high sound absorption at high frequencies as well as the broadband feature in sound absorption. The observed discrepancies can mainly be attributed to the neglected ring

thickness in the FEM model, possible inaccuracy in the air damping estimation, as well as inevitable imperfections in the sample manufacturing and imperfect fitting of the structure to the impedance tube. Nevertheless, the above comparison can verify the FEM model prediction and confirm the superior sound absorption performance of the designed sound absorber through tactic combination of the SBH effects and MPP absorption.

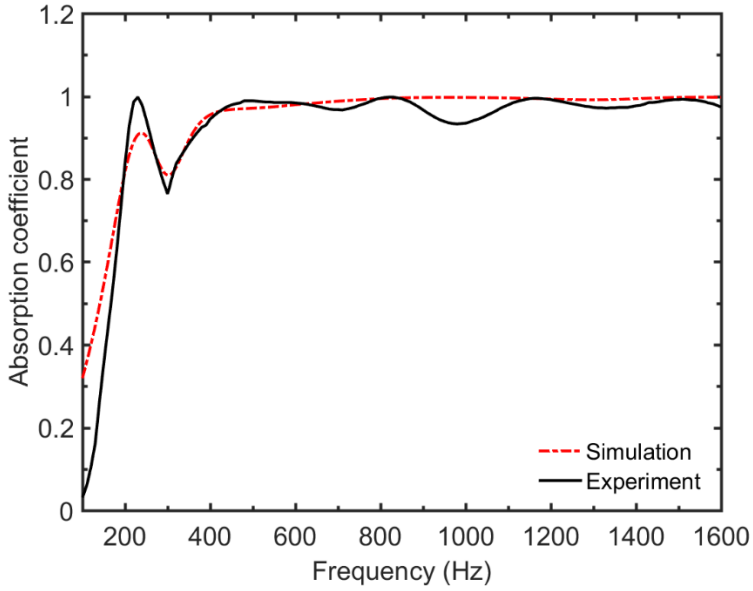

Figure 12: Comparison between measured absorption coefficient and FEM calculations.

5. Conclusions

In summary, we have proposed and numerically and experimentally investigated the design of a sound absorbing device based on the combined SBH and MPP effects. The proposed device excels at low frequencies with a broadband and near perfect sound absorption in the subwavelength thickness region. We demonstrate that the excellent

absorption performance originates from the combined effects of a few important factors: on the top of the list are the ABH-specific wave retarding and energy trapping phenomenon, continuous and space-varying cascade effects of the MPP absorbers and their effective energy dissipation ability. Altogether, acoustic energy is favorably distributed over different MPP portions and get absorbed accordingly by different MPP units, whose effective absorption range is down-shifted to lower frequencies due to SBH-induced reduction in the sound speed. It is also shown that the truncation length at the extremity of the SBH would affect the sound absorption performance mainly in the low-frequency range. The above numerical findings as well as the claimed sound absorption performance are finally confirmed by experiments. The proposed sound absorbers show promise for future applications in noise control engineering.

Acknowledgements

The research reported here was supported by “the Fundamental Research Funds for the Central Universities (WUT: 2021IVA026)”. The authors would like to thank Jiajun Xia for his help in experiments.

References

[1] X. Cai, Q. Guo, G. Hu, J. Yang, Ultrathin low-frequency sound absorbing panels based on coplanar spiral tubes or coplanar Helmholtz resonators, Appl. Phys. Lett., 105 (2014) 121901-121901.

[2] Y. Li, B. Assouar, Acoustic metasurface-based perfect absorber with deep subwavelength thickness, Appl. Phys. Lett., 108 (2016) 063502.

[3] F. Wu, Y. Xiao, D. Yu, H. Zhao, Y. Wang, J. Wen, Low-frequency sound absorption of hybrid absorber based on micro-perforated panel and coiled-up channels, Appl. Phys. Lett., 114 (2019) 151901.

[4] Y. Wang, H. Zhao, H. Yang, J. Zhong, D. Zhao, Z. Lu, J. Wen, A tunable sound-absorbing metamaterial based on coiled-up space, J. Appl. Phys., 123 (2018) 185109.

[5] J.P. Groby, W. Huang, A. Lardeau, Y. Aurégan, The use of slow waves to design simple sound absorbing materials, J. Appl. Phys., 117 (2015).

[6] J.P. Groby, R. Pommier, Y. Aurégan, Use of slow sound to design perfect and broadband passive sound absorbing materials, The Journal of the Acoustical Society of America, 139 (2016) 1660-1671.

[7] N. Jiménez, V. Romero-García, V. Pagneux, J.-P. Groby, Quasi-perfect absorption by sub-wavelength acoustic panels in transmission using accumulation of resonances due to slow sound, Physical Review B, 95 (2016).

[8] N. Jiménez, W. Huang, V. Romero-García, V. Pagneux, J.P. Groby, Ultra-thin metamaterial for perfect and quasi-omnidirectional sound absorption, 109 (2016).

[9] N. Jiménez, V. Romero-García, V. Pagneux, J.-P. Groby, Rainbow-trapping absorbers for transmission problems: Broadband and perfect sound absorbing panels, 2017.

[10] M. Mironov, Propagation of a flexural wave in a plate whose thickness decreases smoothly to zero in a finite interval, Sov. Phys. Acoust., 34 (1988) 318-319.

[11] V.V. Krylov, F.J.B.S. Tilman, Acoustic 'black holes' for flexural waves as effective vibration dampers, J. Sound Vib., 274 (2004) 605-619.

[12] V.V. Krylov, New type of vibration dampers utilising the effect of acoustic 'black holes', Acta Acustica united with Acustica 90 (5) (2004) 830-837.

[13] L. Ma, S. Zhang, and L. Cheng, A 2D Daubechies wavelet model on the vibration of rectangular plates containing strip indentations with a parabolic thickness profile, J. Sound Vib., 429 (2018) 130-146.

[14] J. Deng, L. Zheng, O. Guasch, H. Wu, P. Zeng, and Y. Zuo, Gaussian expansion for the vibration analysis of plates with multiple acoustic black holes indentations, Mech. Syst. Sig. Process., 131 (2019) 317-334.

[15] T. Zhou, J.D. Chazot, E. Perrey-Debain, and L. Cheng, Partition of Unity Finite Element Method for the modelling of Acoustic Black Hole wedges, J. Sound Vib., 475 (2020) 115266.

[16] L. Tang, L. Cheng, H.L. Ji, and J. H. Qiu, Characterization of acoustic black hole effect using a one-dimensional fully-coupled and wavelet-decomposed semi-analytical model, J. Sound Vib., 374 (2016) 172-184.

[17] L. Zhao, Low-frequency vibration reduction using a sandwich plate with periodically embedded acoustic black holes, J. Sound Vib., 441 (2018).

[18] T. Zhou and L. Cheng, A resonant beam damper tailored with Acoustic Black Hole features for broadband vibration reduction, J. Sound Vib., 430 (2018).

[19] L. Ma, L. Cheng, Numerical and experimental benchmark solutions on vibration and sound radiation of an Acoustic Black Hole plate, Appl. Acoust., 163 (2020) 107223.

[20] X. Li, Q. Ding, Sound radiation of a beam with a wedge-shaped edge embedding acoustic black hole feature, J. Sound Vib., 439 (2018).

[21] L. Zhao, S. Conlon, F. Semperlotti, Broadband energy harvesting using acoustic black hole structural tailoring, Smart Mater. Struct., 23 (2014) 065021.

[22] H. Ji, Y. Liang, Y. Wu, Enhancement of vibration based energy harvesting using compound acoustic black holes, Mech. Syst. Sig. Process., 132 (2019) 441-456.

[23] L. Zhao, S. Conlon, F. Semperlotti, An experimental study of vibration based energy harvesting in dynamically tailored structures with embedded acoustic black holes, Smart Mater. Struct., 24 (2015).

[24] A. Pelat, F. Gautier, S. Conlon, F. Semperlotti, The acoustic black hole: A review of theory and applications, J. Sound Vib., 476 (2020) 115316.

[25] M. Mironov, and V. Pislyakov, One-dimensional acoustic waves in retarding structures with propagation velocity tending to zero, Acoust. Phys., 48 (2002) 347-352.

[26] M. Mironov, and V. Pislyakov, One-dimensional sonic black holes: Exact analytical solution and experiments, J. Sound Vib., 473 (2020) 115223.

[27] A. EI-Ouahabi, V.V. Krylov, and D. O'Boy, Investigation of the acoustic black hole termination for sound waves propagating in cylindrical waveguides, in: Proceedings of the Inter-noise and Noise-con Congress and Conference, Institute of Noise Control Engineering, San Francisco, USA, 2015

[28] A. EI-Ouahabi, V. V. Krylove, and D. O'Boy, Experimental investigation of the acoustic black hole for sound absorption in air, in: Proceedings of 22 nd International Congress on Sound and Vibration, Florence, Italy 2015.

[29] O. Guasch, M. Arnela, P. S_anchez-Martín, Transfer matrices to characterize linear and quadratic acoustic black holes in duct terminations, J. Sound Vib., 395 (2017) 65-

79.

[30] O. Guasch, P. Sánchez-Martín, and D. Ghilardi, Application of the transfer matrix approximation for wave propagation in a metafluid representing an acoustic black hole duct termination, Appl. Math. Model., 77 (2020) 1881-1893.

[31] J.P. Hollkamp, and F. Semperlotti, Application of fractional order operators to the simulation of ducts with acoustic black hole terminations, J. Sound Vib., 465.

[32] Y. Mi, W. Zhai, L. Cheng, C. Xi, X. Yu, Wave trapping by acoustic black hole: Simultaneous reduction of sound reflection and transmission, Appl. Phys. Lett., 118 (2021) 114101.

[33] D.-Y. Maa, Potential of microperforated panel absorber, J. Acoust. Soc. Am., 104 (1998) 2861-2866.

[34] D.-Y. Maa, Theory and design of microperforated panel sound-absorbing constructions, Sci. Sin., 18 (1975) 55-71.

[35] X. Zhang, L. Cheng, Acoustic impedance of micro-perforated panels in a grazing flow, J. Acoust. Soc. Am., 145 (2019) 2461-2469.

[36] Y. Tang, S. Ren, H. Meng, F. Xin, L. Huang, T. Chen, C. Zhang, T. Lu, Hybrid acoustic metamaterial as super absorber for broadband low-frequency sound, Sci. Rep., 7 (2017) 43340.

[37] M. Duan, C. Yu, Z. Xu, F. Xin, T. Lu, Acoustic impedance regulation of Helmholtz resonators for perfect sound absorption via roughened embedded necks, Appl. Phys. Lett., 117 (2020) 151904.

[38] M. Duan, C. Yu, F. Xin, T. Lu, Tunable underwater acoustic metamaterials via

quasi-Helmholtz resonance: From low-frequency to ultra-broadband, Appl. Phys. Lett., 118 (2021) 071904.